Data Augmentation based on Inverse Transform Sampling for Improved Tissue Classification via Electrical Impedance Spectroscopy

Conor McDermott
Systems and Computer Engineering
Carleton University
Ottawa, Canada
conormcdermott@cmail.carleton.ca

Carlos Rossa
Systems and Computer Engineering
Carleton University
Ottawa, Canada
rossa@sce.carleton.ca

2023 IEEE Sensors Applications Symposium (SAS) | 979-8-3503-2307-8/23/$31.00 ©2023 IEEE | DOI: 10.1109/SAS58821.2023.10254182

***Abstract*—Ultrasound-guided needle biopsy often leads to uncertain results due to poor visualization of targets in the image. Biopsy needles equipped with electrical impedance spectroscopy (EIS) sensors can be used to identify the tissue at the needle tip and provide more accurate needle guidance and lesion targeting. A machine learning algorithm is often used to classify the tissue based on the measured EIS spectrum. However, training machine learning algorithms requires large amounts of data, which is rarely available in biomedical applications. A solution to increase the size of the dataset and improve the performance of the classifier is to create synthetic data that closely mimics the original measured data.**

This paper proposes inverse transform sampling as a data augmentation method for EIS to bolster training dataset size. It exploits the cumulative distribution functions of the target data and uses inverse sampling to generate new, synthetic data. The method is demonstrated using an EIS dataset composing 13 different *ex-vivo* tissue types. The method is then validated by comparing the performance of the synthetic data to the original data through the use of an artificial neural network (ANN) and a convolutional neural network (CNN). The classification results indicate that classification sensitivity, precision, and accuracy increase by at least 27.38, 24.86, and 19.41%, respectively, when the classifiers used a mix of original data and data augmented with the proposed method.

I. Introduction

Needle biopsies are the gold standard for prostate cancer diagnosis. The biopsy needle is often guided to the lesion of interest by ultrasound (US) imaging. While prostate cancer usually appears as a hypoechoic region in greyscale US, it can also appear as an isoechoic region in up to 30% of cases [1]. As such, guaranteeing proper needle placement and lesion sampling is not always possible until the collected sample is histologically processed, which may result in false-negative outcomes 20% of the time [2]. Furthermore, US-guided biopsies can provide unreliable information on the severity of the lesion, with approximately 30-45% of prostate cancer patients having the status of their diagnosis upgraded following radical prostatectomy [2].

To improve the accuracy of US-guided prostate biopsy, US images are often fused with magnetic resonance imaging (MRI) images [3]. MRI images offer improved resolution of lesions and show lesion boundaries with more clarity as compared to US. MRI-US fusion overlays pre-operative MRI images onto the real-time US images to aid the surgeon in locating and targeting the lesion.

While the clinical pathway for a positive biopsy result is clear, a negative result has an uncertain meaning. A negative result may be due to inaccurate localisation of the lesion due to poor fusion of the MRI and US images, or because the biopsy needle was not inserted into the target adequately. Further, the interpretation of the MRI may be incorrect due to operator error or the presence of other diseases that mimic cancer in MRI. Changes in patient position between the MRI and US imaging may provide poor outcomes for the image fusion [4]. Even considering conventional needle biopsy methods, where 10-15 core samples are taken, surgeons still experience difficulty in capturing representative samples [5]. Therefore, to rule out false negatives, one may consider instrumenting the biopsy needles with sensors that can provide accurate information regarding the composition of the tissue at the tooltip, which can ensure that the needle is placed in the lesion before the tissue is sampled [6]. Such technology can substantially improve the diagnostic yield for targeted biopsy and improve confidence in biopsy results.

Needles instrumented with electrical impedance spectroscopy (EIS) sensors can discriminate tissue composition while maintaining compatibility with the form factor of biopsy needles [7]–[10]. EIS injects AC voltages into the tissue across various frequencies while measuring the resulting AC current, from which the tissue impedance is inferred and used to differentiate tissue [11]. A modified biopsy needle with an EIS sensor that maintained the function of excising samples is shown in [7]. Similarly, the Injeq needle [9] features an

We acknowledge the support of the Natural Sciences and Engineering Research Council of Canada (NSERC), the Canadian Institutes of Health Research (CIHR), and the Social Sciences and Humanities Research Council of Canada (SSHRC), [funding reference number NFRFE-2018-01986].

Cette recherche a été financée par le Conseil de recherches en sciences naturelles et en génie du Canada (CRSNG), par les Instituts de recherche en santé du Canada (IRSC), et par le Conseil de recherches en sciences humaines du Canada (CRSH), [numéro de référence NFRFE-2018-01986]

eccentric electrode geometry that gives the needle highly localised sensitivity [12]–[15]. A hypodermic needle with an EIS sensing circuit manufactured on the needle tip is shown in [16] to discriminate cancerous renal tissue from healthy [17]. The device was also used on *ex-vivo* human thyroids to discern benign tissue and malignancy and presented a sensitivity and specificity of 78.2% and 85.3%, respectively [18]. A quadra-polar EIS sensing probe was used to detect cervical intraepithelial neoplasia (CIN) in [19]. An external use electrical bioimpedance measuring probe for *ex-vivo* prostate cancer detection is presented in [20].

The observed EIS spectra need to be classified to be clinically relevant, and this is often achieved with machine learning algorithms. Classification of EIS spectra falls into two general groups: fitting impedance spectra onto equivalent circuits, and classifying spectra directly. In the first case, an electric circuit is created and the circuit parameters are optimised to match the observed spectra [21], [22]. In the second case, machine learning is often used [7], [20], [23]. While the second option may provide better results than the first [24], [25], the size of the dataset must be sufficiently large to adequately train the classifier. However, due to the time and cost associated with gathering biomedical data, gathering a sufficiently large dataset is difficult and not always feasible.

A. Related work

A common strategy to obtain large quantities of data for classifier training is to synthesise or augment a given dataset. For example, in the field of computer vision, synthetic data is a means of bolstering the size and scope of a training dataset and improving classification performance. While digital images can be skewed, rotated, flipped etc., spectral data, such as in EIS, must maintain their relationship from feature to feature as they are a structured series [26]. Spectral data synthesis has been applied to Raman spectroscopy (RS) to bolster dataset size for clinical classification [27], [28]. Gaussian kernel density estimation was used in [29] to bolster RS spectra for a brain cancer dataset. A statistical method for data augmentation of RS spectra wherein the recorded spectra are altered slightly from the mean value is shown in [30]. Electroencephalogram (EEG) data augmentation has been performed using the addition of *a priori* artifacts and Gaussian white noise to bolster classifier robustness against noise and artifacts [31]. Gaussian white noise is again used in [32] to increase the size of a small EEG training dataset by generating new entries, similar enough to the originals but varied to increase the feature space span. A modified generative adversarial network (GAN) is presented in [33] to bolster EEG training dataset size. Over- and under-sampling have also been applied to EEG datasets to mitigate imbalance during training [34], [35].

While deep learning data augmentation can provide satisfactory synthesis, these methods are often difficult to evaluate. For example, in the case of GANs, tertiary means of evaluation must be implemented, such as the Frechet intercept distance [36]. Variational autoencoders are also difficult to evaluate, oftentimes relying on the performance of a downstream discriminative model. These methods use latent or random variables to generate the entries, and so even statistical evaluation is not an indication of general performance, but rather an indication of the performance of a single run [37]. Further, a deep model's performance strongly depends on the size of the dataset and may collapse during training. Noise addition models are similar in effect to over/under sampling methods and often encourage overfitting. Probabilistic models, on the other hand, allow for a direct model of the data being generated to be exploited. A probabilistic model that requires only knowledge of the mean and standard deviations of the features of an entry may be able to mitigate some of these problems and work with a small-sized dataset.

This paper proposes a statistical data augmentation method based on inverse transform sampling (ITS). It exploits the cumulative distribution functions of the target data and uses inverse sampling to generate new, synthetic data to bolster training dataset size. The proposed model is validated using an EIS dataset acquired using a sensorised biopsy needle and the data augmentation method is evaluated using both an artificial neural network (ANN) and a convolutional neural network (CNN). The classification results indicate that classification metrics are improved when using the proposed data augmentation method with sensitivity, precision, and accuracy increasing by at least 27.38%, 24.86%, and 19.41%, respectively. The method presented is easy to implement, provides good improvements over a baseline without data augmentation, and is less computationally taxing than contemporary deep generative models.

The paper is structured as follows: Section II explains the working principle of EIS for biomedical tissue classification, Section II-A elaborates on the proposed data synthesis method, Section III-A discusses classifiers and metrics for performance evaluation, Section IV presents the classification results with and without synthesised data. Finally, Section V provides a discussion of the results and an overview of future work.

II. Statistical data augmentation for EIS

Before describing the proposed algorithm, it is important to lay out the principles of EIS and how data is collected. In EIS, a voltage $V(j\omega)$ having amplitude V_0, and angular frequency $\omega = 2\pi f$, where f is the excitation frequency in Hz, that is

$$V(t) = V_0 \sin(\omega t), \tag{1}$$

where t is the time, is applied to the tissue sample. If the tissue's frequency-dependent impedance $Z(j\omega)$ is

$$Z(j\omega) = R + Y(j\omega), \tag{2}$$

where R is the electrical resistance and $Y(j\omega)$ is the reactance, with $j = \sqrt{-1}$, then the current induced in the sample is

$$I(t) = I_0 \sin(\omega t + \theta) = \frac{V(j\omega)}{Z(j\omega)} \tag{3}$$

where I_0 is the current magnitude and θ is the phase shift of the current relative to the voltage. From the above, the

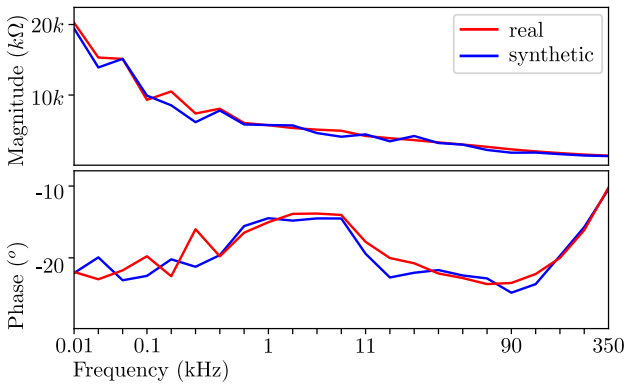

Fig. 1. A comparison of measured and synthesised spectra.

magnitude and phase of the tissue's impedance at a frequency ω are

$$|Z(\omega)| = \sqrt{R^2 + Y^2}, \tag{4}$$

$$\theta = -\arctan\left(\frac{Y}{R}\right). \tag{5}$$

The objective of EIS is to collect the phase and magnitude of the tissue's impedance at a discrete number of frequencies and classify the tissue type based on this information.

A. Data synthesis from inverse transform sampling

In this paper, samples are grouped by their class, c, e.g., chicken liver, bovine muscle, etc. A feature x of a given class is either the phase or the magnitude of sample c's impedance at a given frequency. If each feature is measured n times, the spectral data of class c, that is X_c, is structured as:

$$X_c = \begin{bmatrix} x_{1,1} & x_{1,2} & \dots & x_{1,m} \\ x_{2,1} & x_{2,2} & \dots & x_{2,m} \\ \vdots & \vdots & \ddots & \vdots \\ x_{n,1} & x_{n,2} & \dots & x_{n,m} \end{bmatrix}$$

where $x_{i,k}$ is the i^{th} unique entry, $i \in [1, n]$, of the k^{th} feature, $k \in [1, m]$. In this structure, each column of X_c has all the magnitude or phase measurements of given a frequency, and each row has all features from a given measurement.

The means and standard deviation of each class are calculated as:

$$\mu_k = \frac{1}{n}\sum_{i=1}^{n} x_{i,k} \tag{6}$$

and

$$\sigma_k = \sqrt{\frac{1}{n}\sum_{i=1}^{n}(x_{i,k} - \mu_k)^2}. \tag{7}$$

A Gaussian cumulative distribution function having the same mean and standard deviations calculated above is then created at each frequency to create new, synthetic data entries. It is assumed that the entries of each feature adhere to a Gaussian distribution, and are monotonically increasing.

A vector $r \sim \mathcal{N}(0, 1)$ of normally distributed random points is first generated. The relative likelihood associated with a value of r is found using the Gaussian cumulative distribution function,

$$p = F_r(r) = \frac{1}{2}\left[1 + \text{erf}\left(\frac{r}{\sqrt{2}}\right)\right], \tag{8}$$

where F_r is the cumulative density function of r and $F_r : \mathbb{R} \to [0, 1]$, r is the point at which the probability is being calculated, p is the probability of r, and erf is the error function:

$$\text{erf}(x) = \frac{2}{\sqrt{\pi}}\int_0^x e^{-t^2} dt.$$

The inverse of the cumulative distribution function, also known as the percent point function or the quantile function, shown as $Q = F_r^{-1} : [0, 1] \to \mathbb{R}$, can be used to take the probabilities of the random, normally distributed variable and determine the equivalent values in the domain of k. The quantile function of the feature, Q_m, can be generated and used to translate the $F_r(r)$ to the domain of k as

$$g = Q_k(p) = F_k^{-1}(p) \tag{9}$$

where g is the translated random entries. Following this transformation, $g \sim \mathcal{N}(\mu_k, \sigma_k)$. These new entries will appear similar to those of the original entries as they exist in the same probability distribution, but as each frequency is considered independent, the covariance of features is lost. Further, as the random points used to generate new entries and normally distributed, their translations will too be normally distributed, which may not be the case for the original data.

An example of the statistically synthesised data compared to original data is shown in figure 1, and a plot showing the statistical distribution congruency and translation between the original and synthesised data domains for a single feature of a single class at a single frequency is shown in figure 2. A pseudocode representation of the statistical data synthesiser is shown in Algorithm 1.

Algorithm 1 ITS data augmentation data algorithm

for m **do** ▷ Find statistical representation of each feature
  $\mu_k = \text{mean}(x_{i,k}) \forall i \in n$
  $\sigma_m = \text{stddev}(x_j) \forall i \in n$
  $r \sim \mathcal{N}(0, 1)$
  $p = F_r(r) : \mathbb{R} \to [0, 1]$
  $g = Q_k(p) = F_k^{-1}(p) : [0, 1] \to \mathbb{R}$
end for

The synthetic data is statistically identical to the original data and maintains its representation of the feature space. Synthetic data can be created to bolster the size of the training dataset and still be representative of the original feature space.

III. Experimental Validation

A. Data collection

A sensorised needle in bipolar configuration is used for EIS measurements of various tissue samples. The needle is

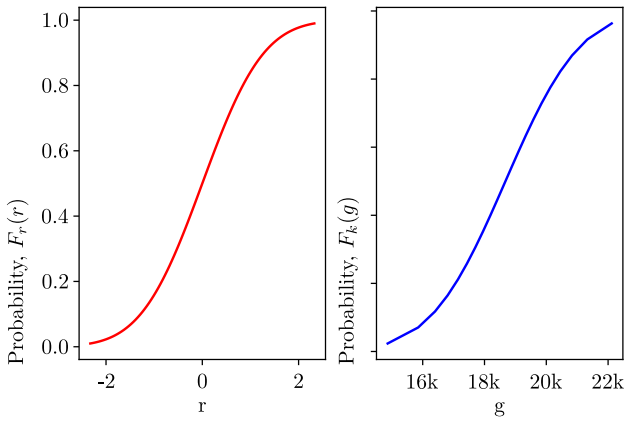

Fig. 2. Original and synthesised cumulative density function for one feature of one class. The left x axis shows the distribution of a randomly generated variable, and the x axis on the right shows the distribution of a given feature of a given class. The y-axes show the probability distribution of the variable in question.

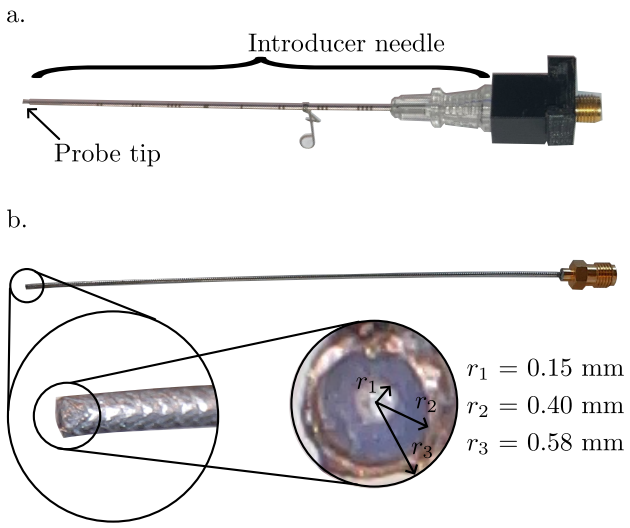

Fig. 3. In (a) the Sensorised electrode in the introducer needle. In (b) the sensorised electrode with macro shots of the needle tip showing the coaxial electrode configuration.

composed of a coaxial cable electrode (Mouser, model 095-902-462-009) inserted in a rigid surgical introducer needle (Argon Medical Devices, model MCXS1815LX), figure 3a. The coaxial cable has an inner diameter of 0.30 mm and an outer diameter of 1.16 mm, see the right side of figure 3b. The woven shielding of the coaxial cable acts as the outer electrode, and the inner cable as the inner electrode. The electrodes have a separation distance of approximately 0.35 mm.

The needle is connected to an impedance spectroscopy system (Eliko, model Quadra impedance spectroscopy analyzer). A set of 23 frequencies spaced from 0.01 to 350 kHz are used for the measurements. At each frequency, the resultant magnitude and phase change are measured. Collection of the *ex-vivo* animal tissue data is outlined in [24].

The original dataset is composed of 13 different tissue types. For each tissue, between 14 and 22 measurements are taken, totalling 246 spectra. This data is split into two subsets, a training set, and a test set. The original training set serves two purposes: it is used as the input to the data augmentation algorithm and to train the classifiers described later. The test set is held out and only used to evaluate the accuracy of the classifiers following training.

In addition, 325 new spectra are created for each of the 13 tissue classes using the data synthesis method outlined above. These are split into a synthesised training set of 250 spectra, and a validation set of 75 spectra. Thus, there are a total of 4 datasets of varying combinations of spectra. Each has 3 subsets of data: a train set to train the network, a validation set to validate the model during training, and a test set to evaluate the model after training.

- **Dataset 1 (DS1)**: 103 original to train, 43 original to validate, and 103 original to test the model;
- **Dataset 2 (DS2)**: 143 original and 2250 synthesised to train, 975 synthesised to validate, and 103 original to test the model;
- **Dataset 3 (DS3)**: 103 original and 2250 synthesised to train, 43 original and 975 to validate, and 103 original to test the model;
- **Dataset 4 (DS4)**: 2250 synthesised to train, 975 synthesised to validate, and 103 original to test the model.

DS1 is used to train and evaluate the classifiers without augmented data and serves as a baseline. When augmented data is used, the classifiers are retrained and reevaluated using datasets DS2, DS3, and DS4. The variations between these 3 datasets will show how well the synthesised data can generalise to the original data.

B. Classification algorithms

The quality of a synthesised training dataset can be evaluated by comparing the performance of a classifier trained on the original data to a classifier trained on the synthesised data. In this paper, effectiveness of the proposed algorithm is evaluated through an artificial neural network (ANN), and a 1-dimension convolutional neural network (CNN). Both classifiers are trained on the original data alone and then separately with the augmented data.

The ANN is composed of 3 layers: a dense layer with 100 units and ReLU activation, a dense layer with 1000 units, ReLU activation, and a dropout function with probability 0.2, and a third dense layer with 13 units and softmax activation.

The CNN consists of a convolutional layer with 128 filters, batch normalization, max pooling, and leaky ReLU activation. Next, a flatten layer is followed by a dense layer with 100 units, batch normalization, dropout with a probability of 0.2, and leaky ReLU activation. Lastly, decisions are made with a dense layer with 13 units and softmax activation, shown in figure 4. Both classifiers are trained using the same computer (Intel, model i5-8350U at 1.7 GHz) for a maximum of 1000 epochs, use Adam optimisation, and sparse categorical cross-entropy for loss. The most accurate model with the highest validation accuracy is saved and evaluated on the test dataset.

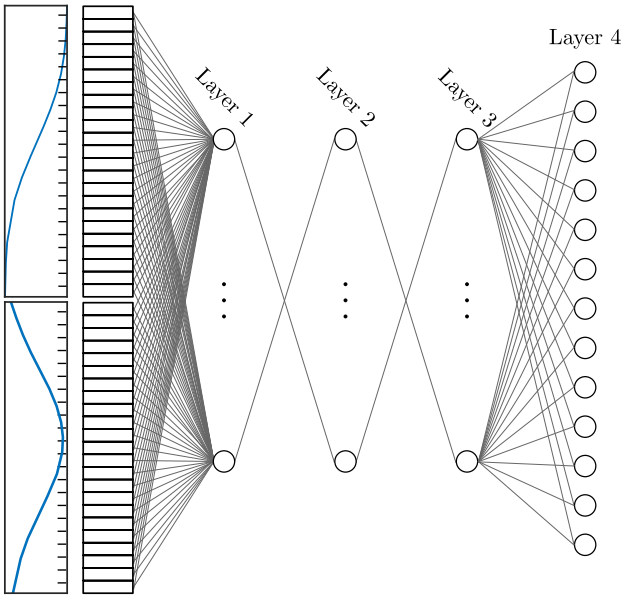

Fig. 4. CNN structure. Layer 1: Convolutional layer with batch normalization, max pooling, and leaky ReLU activation. Layer 2: Flatten layer. Layer 3: Dense layer with batch normalization, dropout, and leaky ReLU activation. Layer 4: Dense layer with Softmax activation.

TABLE I
CLASSIFIER TRAINING PERFORMANCE

Classifier	Dataset	Training time (s)	Validation accuracy (%)
ANN	DS1	31.9	20.7
	DS2	274.3	99.8
CNN	DS1	42.7	24.1
	DS2	568.1	99.7

Metrics for evaluating classifier performance are sensitivity, precision, and accuracy.

IV. EXPERIMENTAL RESULTS

The two classifiers' training performances are compared in Table I. Both classifiers take approximately 10 times longer to train when using the augmented data, which is a reasonable trade-off as the synthesised data set is approximately 20 times larger than the original dataset.

Table II summarises the classification results using the original and augmented data with both the ANN and CNN classifiers. The ANN with the original data, DS1, shows sensitivity, precision, and accuracy of 53.57%, 51.41%, and 63.11%, respectively. Using the DS2 data configuration on a retrained model, these metrics increase by 27.38%, 24.86%, and 19.41%. The DS3 configuration, which includes some original data in the validation set, provides a sensitivity, precision, and accuracy of 81.88%, 76.56%, and 83.50%, an even larger increase. DS4, which uses only synthesised data gives a sensitivity, precision, and accuracy of 77.36%, 71.23%, and 78.64%, which is a significant improvement over the original dataset alone.

The CNN trained only on original data, DS1, shows sensitivity, precision, and accuracy of 53.01%, 40.24%, and 49.51%,

TABLE II
CLASSIFIER ACCURACY (%) FOR DIFFERENT COMBINATIONS OF TRAINING, VALIDATION, AND TEST DATASETS (DS)

Classifier	Dataset	Sensitivity	Precision	Accuracy
ANN	DS 1	53.57	51.41	63.11
	DS 2	80.95	76.27	82.52
	DS 3	81.88	76.56	83.50
	DS 4	77.36	71.23	78.64
CNN	DS 1	53.01	40.24	49.51
	DS 2	81.98	75.23	82.52
	DS 3	**83.02**	**78.67**	**84.47**
	DS 4	70.82	68.05	71.84

respectively, and these metrics increase to 81.98%, 75.23%, and 82.52% with the DS 2 configuration. The CNN trained on the DS3 configuration gives 83.02%, 78.67%, and 84.47% for sensitivity, precision, and accuracy. The use of original and synthetic data in training and validation thus increases sensitivity, precision, and accuracy by 30.01%, 38.43%, and 34.96%, respectively. Evaluating the CNN on the DS4 configuration gives a sensitivity, precision, and accuracy of 70.82%, 68.05%, and 71.84%.

In both the ANN and CNN classifiers, the augmented data increases the sensitivity significantly. After training, both the ANN and CNN are capable of real-time classification, providing predictions for a single entry in 20 ms and 17 ms, respectively.

V. DISCUSSION AND CONCLUSION

Using inverse sampling for data synthesis to increase the small sample size of EIS measurements for tissue classification has been shown to be effective. Important metrics for clinical classification such as sensitivity see at least a 15% increase relative to baseline. The synthesised data can be seen to be effective as training a model only on the synthesised data, DS4, allows the network to perform better than training the model only on original data. It seems that providing some original data to the train set and some to the validation set, DS3, provides the best results overall, with both the CNN and ANN scoring the best in this configuration. Using no original data in the validation set, DS2, performs almost as well as DS3 and should also be considered. A further comparison can be made to [24] wherein only the original data is used, equivalent to DS1. In that publication, the highest sensitivity obtained was 80.58%. In most cases, the ANN and CNN provided here using synthesised data match or beat that value, indicating good performance and an improvement over baseline.

The data synthesis method presented in this paper is simple to implement, requiring only a Gaussian cumulative distribution representation of the data to be synthesised. It is limited in terms of its ability to create data not represented by the original dataset, but this is an issue that befell most data synthesis methods. Further, it does not maintain the relationship between features covariance's, which may lead to poor feature space representation. However, machine learning methods provided with training data synthesised using this method significantly

outperform the equivalent models when they are not provided with synthetic data.

In terms of biomedical applications of EIS, the limitations on data collection for training classifiers compromise the accuracy of the machine learning algorithms used for classification. The results presented in this paper show that a neural network trained on feature space expanding EIS sensorised biopsy needle synthetic data can better classify *ex-vivo* animal tissue better than one not trained with synthetic data.

REFERENCES

[1] A. Ebeid and A. Elshamy, "Hypoechoic versus hypervascular lesion in the diagnosis of prostatic carcinoma," *African Journal of Urology*, vol. 24, no. 3, pp. 169–174, 2018.

[2] J. S. Quon, B. Moosavi, M. Khanna, T. A. Flood, C. S. Lim, and N. Schieda, "False positive and false negative diagnoses of prostate cancer at multi-parametric prostate mri in active surveillance," *Insights into imaging*, vol. 6, no. 4, pp. 449–463, 2015.

[3] L. Marks, S. Young, and S. Natarajan, "Mri–ultrasound fusion for guidance of targeted prostate biopsy," *Current opinion in urology*, vol. 23, no. 1, p. 43, 2013.

[4] M. Kongnyuy, A. K. George, A. R. Rastinehad, and P. A. Pinto, "Magnetic resonance imaging-ultrasound fusion-guided prostate biopsy: review of technology, techniques, and outcomes," *Current urology reports*, vol. 17, pp. 1–9, 2016.

[5] G. J. Kelloff, P. Choyke, and D. S. Coffey, "Challenges in clinical prostate cancer: role of imaging," *AJR. American journal of roentgenology*, vol. 192, no. 6, p. 1455, 2009.

[6] M. Kaneko, D. Sugano, A. H. Lebastchi, V. Duddalwar, J. Nabhani, C. Haiman, I. S. Gill, G. E. Cacciamani, and A. L. Abreu, "Techniques and outcomes of mri-trus fusion prostate biopsy," *Current urology reports*, vol. 22, pp. 1–12, 2021.

[7] V. Mishra, H. Bouayad, A. Schned, A. Hartov, J. Heaney, and R. J. Halter, "A real-time electrical impedance sensing biopsy needle," *IEEE transactions on biomedical engineering*, vol. 59, no. 12, pp. 3327–3336, 2012.

[8] P. Héroux and M. Bourdages, "Monitoring living tissues by electrical impedance spectroscopy," *Annals of biomedical engineering*, vol. 22, pp. 328–337, 1994.

[9] S. Halonen, J. Kari, P. Ahonen, K. Kronström, and J. Hyttinen, "Real-time bioimpedance-based biopsy needle can identify tissue type with high spatial accuracy," *Annals of biomedical engineering*, vol. 47, no. 3, pp. 836–851, 2019.

[10] V. Mishra, A. Schned, A. Hartov, J. Heaney, J. Seigne, and R. Halter, "Electrical property sensing biopsy needle for prostate cancer detection," *The Prostate*, vol. 73, no. 15, pp. 1603–1613, 2013.

[11] J. Jossinet, "The impedivity of freshly excised human breast tissue," *Physiological measurement*, vol. 19, no. 1, p. 61, 1998.

[12] S. Halonen, J. Kari, P. Ahonen, T. Elomaa, P. Annus, and K. Kronstrom, "Biopsy needle including bioimpedance probe with optimized sensitivity distribution," *Int. J. Bioelectromagn.*, vol. 17, no. 1, pp. 26–30, 2015.

[13] S. Halonen, K. Annala, J. Kari, S. Jokinen, A. Lumme, K. Kronström, and A. Yli-Hankala, "Detection of spine structures with bioimpedance probe (bip) needle in clinical lumbar punctures," *Journal of Clinical Monitoring and Computing*, vol. 31, pp. 1065–1072, 2017.

[14] H. Sievänen, J. Kari, S. Halonen, T. Elomaa, O. Tammela, H. Soukka, and V. Eskola, "Real-time detection of cerebrospinal fluid with bioimpedance needle in paediatric lumbar puncture," *Clinical Physiology and Functional Imaging*, vol. 41, no. 4, pp. 303–309, 2021.

[15] H. A. Bidgoli, N. Schieda, and C. Rossa, "On the sensitivity of bevelled and conical coaxial needle probes for dielectric spectroscopy," *IEEE Transactions on Instrumentation and Measurement*, vol. 72, p. 8002209, 2023.

[16] J. Yun, G. Kang, Y. Park, H. W. Kim, J.-J. Cha, and J.-H. Lee, "Electrochemical impedance spectroscopy with interdigitated electrodes at the end of hypodermic needle for depth profiling of biotissues," *Sensors and Actuators B: Chemical*, vol. 237, pp. 984–991, 2016.

[17] J. Yun, H. W. Kim, Y. Park, J.-J. Cha, J. Z. Lee, D. G. Shin, and J.-H. Lee, "Micro electrical impedance spectroscopy on a needle for ex vivo discrimination between human normal and cancer renal tissues," *Biomicrofluidics*, vol. 10, no. 3, p. 034109, 2016.

[18] J. Yun, Y.-T. Hong, K.-H. Hong, and J.-H. Lee, "Ex vivo identification of thyroid cancer tissue using electrical impedance spectroscopy on a needle," *Sensors and Actuators B: Chemical*, vol. 261, pp. 537–544, 2018.

[19] S. Abdul, B. Brown, P. Milnes, and J. Tidy, "The use of electrical impedance spectroscopy in the detection of cervical intraepithelial neoplasia," *International Journal of Gynecologic Cancer*, vol. 16, no. 5, 2006.

[20] R. J. Halter, A. Hartov, J. A. Heaney, K. D. Paulsen, and A. R. Schned, "Electrical impedance spectroscopy of the human prostate," *IEEE Transactions on Biomedical Engineering*, vol. 54, no. 7, pp. 1321–1327, 2007.

[21] A. S. Elwakil, A. A. Al-Ali, and B. J. Maundy, "Extending the double-dispersion cole–cole, cole–davidson and havriliak–negami electrochemical impedance spectroscopy models," *European Biophysics Journal*, vol. 50, no. 6, pp. 915–926, 2021.

[22] O. Casas, R. Bragos, P. Riu, J. Rosell, M. Tresanchez, M. Warren, A. Rodriguez-Sinovas, A. Carreno, and J. Cinca, "In vivo and in situ ischemic tissue characterization using electrical impedance spectroscopy a," *Annals of the New York Academy of Sciences*, vol. 873, no. 1, pp. 51–58, 1999.

[23] Z. Cheng, A. L. C. Carobbio, L. Soggiu, M. Migliorini, L. Guastini, F. Mora, M. Fragale, A. Ascoli, S. Africano, D. G. Caldwell *et al.*, "Smartprobe: a bioimpedance sensing system for head and neck cancer tissue detection," *Physiological measurement*, vol. 41, no. 5, p. 054003, 2020.

[24] B. Kent and C. Rossa, "Tissue discrimination from impedance spectroscopy as a multi-objective optimisation problem with weighted naïve bayes classification," in *2020 IEEE International Conference on Systems, Man, and Cybernetics (SMC)*. IEEE, 2020, pp. 321–327.

[25] ——, "Electric impedance spectroscopy feature extraction for tissue classification with electrode embedded surgical needles through a modified forward stepwise method," *Computers in Biology and Medicine*, vol. 135, p. 104522, 2021.

[26] C. Mandal and R. Zimmer, "A genetic algorithm for the synthesis of structured data paths," in *VLSI Design 2000. Wireless and Digital Imaging in the Millennium. Proceedings of 13th International Conference on VLSI Design*. IEEE, 2000, pp. 206–211.

[27] M. Wu, S. Wang, S. Pan, A. C. Terentis, J. Strasswimmer, and X. Zhu, "Deep learning data augmentation for raman spectroscopy cancer tissue classification," *Scientific reports*, vol. 11, no. 1, p. 23842, 2021.

[28] S. Yu, H. Li, X. Li, Y. V. Fu, and F. Liu, "Classification of pathogens by raman spectroscopy combined with generative adversarial networks," *Science of The Total Environment*, vol. 726, p. 138477, 2020.

[29] Q. Li, J. Wang, and Y. Zhou, "Data augmentation method based on the gaussian kernel density for glioma diagnosis with raman spectroscopy," *Analytical Methods*, 2023.

[30] E. J. Bjerrum, M. Glahder, and T. Skov, "Data augmentation of spectral data for convolutional neural network (cnn) based deep chemometrics," *arXiv preprint arXiv:1710.01927*, 2017.

[31] R. Hussein, H. Palangi, R. Ward, and Z. J. Wang, "Epileptic seizure detection: A deep learning approach," *arXiv preprint arXiv:1803.09848*, 2018.

[32] E. S. Salama, R. A. El-Khoribi, M. E. Shoman, and M. A. W. Shalaby, "Eeg-based emotion recognition using 3d convolutional neural networks," *International Journal of Advanced Computer Science and Applications*, vol. 9, no. 8, 2018.

[33] X. Zhang, Z. Wang, D. Liu, and Q. Ling, "Dada: Deep adversarial data augmentation for extremely low data regime classification," in *Icassp 2019-2019 ieee international conference on acoustics, speech and signal processing (icassp)*. IEEE, 2019, pp. 2807–2811.

[34] R. Manor and A. B. Geva, "Convolutional neural network for multi-category rapid serial visual presentation bci," *Frontiers in computational neuroscience*, vol. 9, p. 146, 2015.

[35] P. Thodoroff, J. Pineau, and A. Lim, "Learning robust features using deep learning for automatic seizure detection," in *Machine learning for healthcare conference*. PMLR, 2016, pp. 178–190.

[36] Q. Xu, G. Huang, Y. Yuan, C. Guo, Y. Sun, F. Wu, and K. Weinberger, "An empirical study on evaluation metrics of generative adversarial networks," *arXiv preprint arXiv:1806.07755*, 2018.

[37] R. C. Pereira, M. S. Santos, P. P. Rodrigues, and P. H. Abreu, "Reviewing autoencoders for missing data imputation: Technical trends, applications and outcomes," *Journal of Artificial Intelligence Research*, vol. 69, pp. 1255–1285, 2020.